Wenxuan Jia
Department of Aerospace and Mechanical Engineering,
University of Southern California,
Los Angeles, CA 90089-1057
e-mail: wenxuanj@mit.edu

Yuen-Shan Leung
Daniel J. Epstein Department of Industrial and Systems Engineering,
University of Southern California,
Los Angeles, CA 90089-1057
e-mail: debbieleung22@gmail.com

Huachao Mao
School of Engineering Technology,
Purdue University,
West Lafayette, IN 47907-2021
e-mail: mao145@purdue.edu

Han Xu
Daniel J. Epstein Department of Industrial and Systems Engineering,
University of Southern California,
Los Angeles, CA 90089-1057
e-mail: hxu050@usc.edu

Chi Zhou
Department of Industrial and Systems Engineering,
University at Buffalo,
Buffalo, NY 14260
e-mail: chizhou@buffalo.edu

Yong Chen[1]
Daniel J. Epstein Department of Industrial and Systems Engineering,
University of Southern California,
Los Angeles, CA 90089-1057
e-mail: yongchen@usc.edu

Hybrid-Light-Source Stereolithography for Fabricating Macro-Objects With Micro-Textures

Microscale surface structures are commonly found on macroscale bodies of natural creatures for their unique functions. However, it is difficult to fabricate such multi-scale geometry with conventional stereolithography processes that rely on either laser or digital micromirror device (DMD). More specifically, the DMD-based mask projection method displays the image of a cross section of the part on the resin to fabricate the entire layer efficiently; however, its display resolution is limited by the building area. In comparison, the laser-based vector scanning method builds smooth features using a focused laser beam with desired beam-width resolution; however, it has less throughput for its sequential nature. In this paper, we studied the hybrid-light-source stereolithography process that integrates both optical light sources to facilitate the fabrication of macro-objects with microscale surface structures (called micro-textures in the paper). The hardware system uses a novel calibration approach that ensures pixel-level dimensional accuracy across the two light sources. The software system enables designing the distribution and density of specific microscale textures on a macro-object by generating projection images and laser toolpaths for the two integrated light sources. Several test cases were fabricated to demonstrate the capability of the developed process. A large fabrication area (76.8–80.0 mm) with 50 μm micro-features can be achieved with a high throughput. [DOI: 10.1115/1.4051831]

Keywords: modeling and simulation, additive manufacturing, stereolithography, texture, multiscale

1 Introduction

Nature has inspired engineers with complex, yet effective surface structures with special mechanical and dynamical functions that are well adapted to the natural environment. For example, shark skin is a well-known example that illustrates the use of micro-structures to improve hydrodynamic performance. Patterns of microscale denticles on the shark's streamlined body are capable of creating greater leading-edge vortices than the perfectly smooth surface, reducing the drag force of the fluid [1,2]. Another well-known example is lotus leaves (Figs. 1(*a*) and 1(*b*)), which possess superhydrophobic property through the multicellular trichomes structure [3]. In comparison, hook structures formed with hairs (Figs. 1(*c*) and 1(*d*)) are found on the shoot of common bean to enhance its adhesion for climbing [4]. Both creatures benefit from integrating microscale structures to their macroscale body. The capability of biomimicking these structures would help the developments of new engineering components with extraordinary functions. However, how to effectively and efficiently fabricate such macro-objects with microscale surface structures (called micro-textures in the paper) is a key problem to be addressed, which is the focus of this paper.

It is difficult for the traditional manufacturing processes such as milling or injection molding to fabricate macroscale objects with complex micro-structures. Additive manufacturing (AM), in contrast, is a novel manufacturing technology that can fabricate three-dimensional (3D) objects through the layer-based accumulation of two-dimensional (2D) layers, regardless of 3D objects' shape complexity. Thus, AM technology has been increasingly used in exploring biomimetic applications due to its fast fabrication and the enabled geometric design freedom [5,6]. Among various types of AM processes, vat photopolymerization such as stereolithography (SL) has become one of the most commonly used AM processes due to its high accuracy and resolution [7]. In the SL process, each layer is fabricated by photopolymerizing a thin film of liquid resins at designated *XY* positions, and a set of 2D layers are accumulated in the *Z*-direction to form a 3D object.

Based on the light source to cure liquid resin into a solid part, current SL processes can be classified as the projection-based and the laser scanning-based approaches. The projection-based SL uses a digital micromirror device (DMD) or a liquid crystal display as the energy source by controlling the light of each pixel on or off. When a pixel is turned on, the photosensitive resin at the position of the pixel is cured. Accordingly, a set of pre-computed image patterns can be displayed sequentially to fabricate

[1]Corresponding author.

Manuscript received July 3, 2021; final manuscript received July 14, 2021; published online August 6, 2021. Tech. Editor: Y. Lawrence Yao.

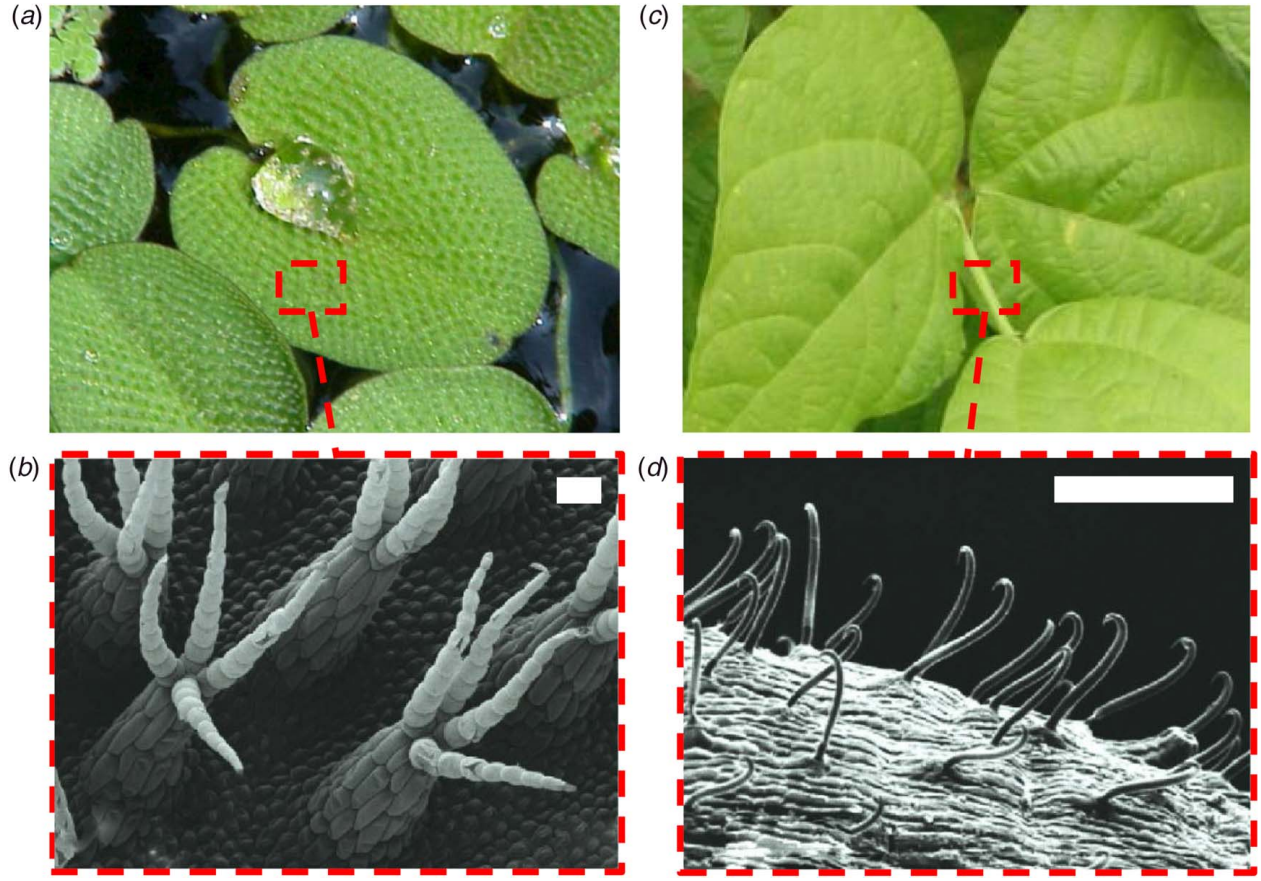

Fig. 1 Functional micro-features found on bodies of creatures. (*a*) The shoot of a lotus (*Salvinia minima*) leaf with (*b*) multicellular hair of four trichomes from a common base (Ref. [4]). (c) The shoot of a common bean (*Phaseolus vulgaris*) with (*d*) terminal hook structures (Ref. [4]). The scale bar is 200 μm. (Creative Commons Attribution 4.0 International (CC BY 4.0))

a 3D object. The resolution of the projection-based SL method heavily depends on the building area. In comparison, the laser scanning-based SL method achieves the resolution by focusing the laser beam into a small spot size. Since resin is cured only at the beam spot sequentially, the laser scanning method is slower than the projection-based SL method. Such inherent trade-offs among the fabrication area, speed, and resolution exist in all the single light source-based SL processes. For example, enlarging the fabrication area of the projection-based SL would inevitably reduce the fabrication resolution due to the limited number of pixels in a DMD, and vice versa.

Many approaches have been developed to address such trade-offs. For example, the scanning projection SL process expands the fabrication area by moving the projector source in the *XY*-directions. During each grid of projection, the resolution can be shrunk to microscale and it would take multiple times of exposure to fabricate a single layer of a macro-object. The projection micro-stereolithography process is capable of fabricating microscopic features [8,9]; however, its fabrication size is usually limited to several millimeters [10–12]. Similarly, direct laser writing only achieves the nanoscale resolution within an area of hundreds of μm^2 [13,14]. Directional SL accumulation has the capability of fabricating micro-features with relatively larger size constraints [15,16]. However, it requires much effort to align the immersed guide tool with the pre-fabricated part to build individual micro-features. All these methods managed to enhance the building area or resolution by manipulating light source, but the inherent trade-offs still exist that make the fabrication of a macroscale object with microscale structures challenging.

Zhou et al. established the concept of the hybrid-source SL method and developed an image-based systematic slicing and toolpath planning algorithm from software perspective [17,18]. However, only the laser toolpath of the contour was planned whereas a computer-aided design (CAD) system for designing general textures is desired. Multi-scale laser-based SL methods using different beam sizes have also been developed, but the efficiency of laser scanning is still limited by its sequential nature [19,20]. Recently, Busetti et al. studied the hybrid-source SL method on improving the surface quality of the fabricated objects [21]. In comparison, our research focuses on how to use the hybrid-source SL process to fabricate macroscale objects with microscale surface structures.

In this paper, a multi-scale AM method based on a hybrid-light-source SL process is presented to fabricate macroscale objects with microscale textures. The process can enhance the fabrication resolution without sacrificing building speed, which is especially suitable to fabricate large objects with microscale features. The key challenges in the integration of hybrid light sources are discussed. The demonstrated hybrid-light-source method is shown in Fig. 2, which synergistically integrates both laser and DMD to facilitate the fabrication of multi-scale features. The fabrication results proved that the developed hybrid-light-source process can achieve high-resolution without sacrificing efficiency. The main contributions of the paper are:

(1) Developed a hybrid-source SL process with a robust calibration method that can ensure both light sources with desired dimensional accuracy.
(2) Presented a fabrication strategy with a generalized CAD tool that enables the design and fabrication of micro-structures and their distributions on a solid model with high fabrication efficiency.

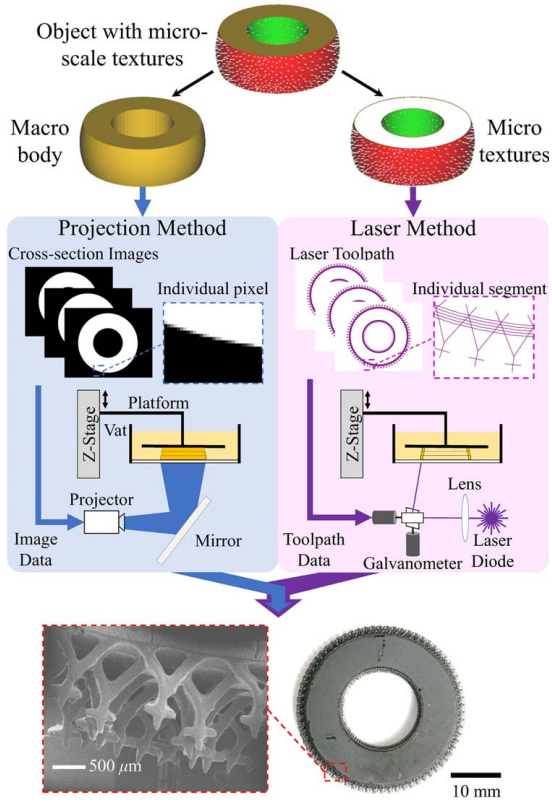

Fig. 2 Dividing the fabrication of a macroscale solid body and microscale structures on its surfaces using the projection-based and laser-based SL methods. A developed CAD tool designs the distribution and density of the microscale textures. The SEM image shows the fabricated triangle-cross feature on the ring-shaped body. The left side is associated with projection and the right side shows the laser toolpath (the same color schemes are used throughout the paper). Note that only different light sources were used in its fabrication. The wavelength of both light sources is the same (405 nm).

(3) Demonstrated the capability and limitations of the hybrid-source SL process on fabricating various complex micro-structures on the surface of a solid object.

The rest of this paper is organized as follows. Section 2 presents the overall hardware design and the calibration process of both light sources. Section 3 discusses the fabrication strategy and the generation of projection images and laser toolpath for both macroscale objects and microscale structures. The process planning of the multi-scale hybrid SL process is also discussed in Sec. 3. Experimental results and process characterization are presented in Sec. 4. Finally, conclusions with future work are drawn in Sec. 5.

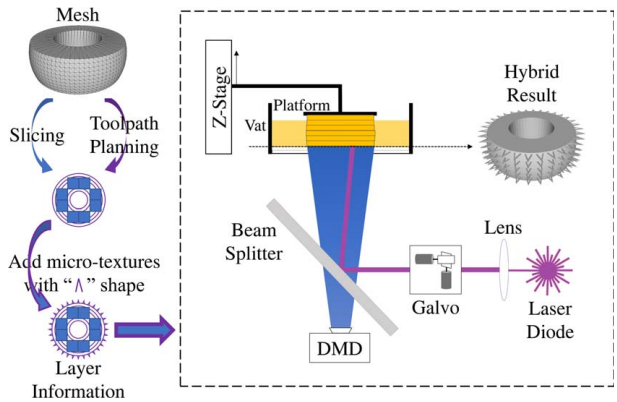

Fig. 3 Schematic diagram and information flow of the hybrid-light-source SL system. A beam splitter was used to combine the optical paths of both energy sources. The laser beam width and micro-structures are exaggerated in the diagram and not to scale.

2 Process Setup and Hardware System Design

2.1 Process Characterization. The hybrid-light-source SL process essentially integrates two distinctive light sources, a laser and a DMD. Each of the light source and the related control has their advantages and disadvantages.

The DMD-based mask image projection method is easy to configure with good reliability. The on/off states of each pixel can be controlled at any time by pipelining a series of images to the DMD-based projector, selectively curing the portion of resin defined by each mask image. The focus of each pixel shares the

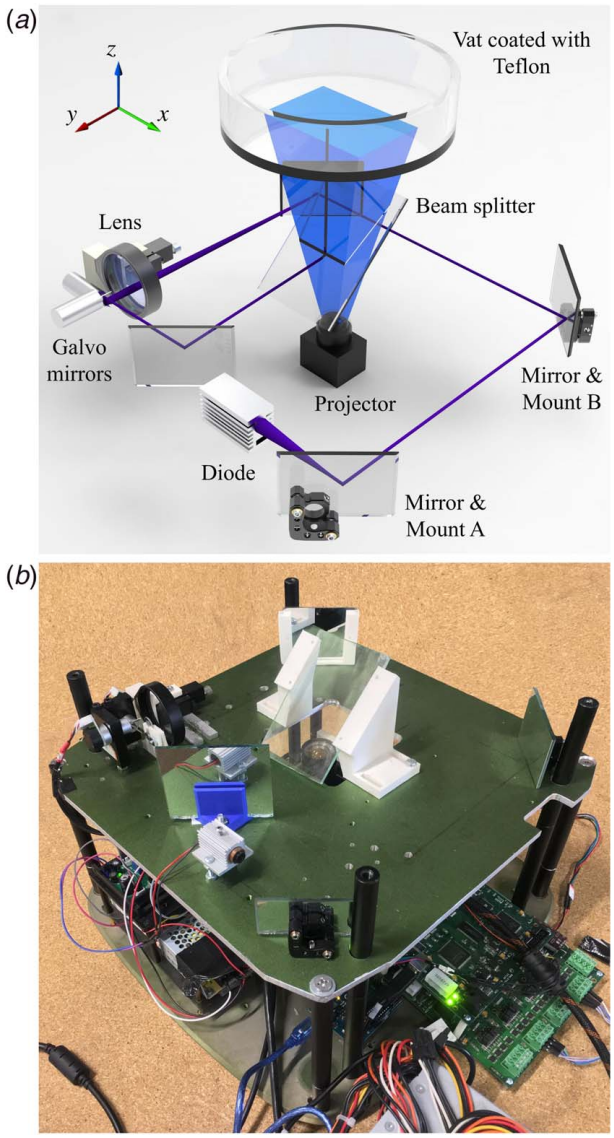

Fig. 4 Illustrations of (*a*) machine design and (*b*) the actual prototype of the hybrid-light-source SL system with key components and machine coordinate system annotated. Note that the mirrors are drawn transparent to illustrate the laser path, and the *Z*-direction linear stage is omitted in the diagram to show the optical paths of the two light sources.

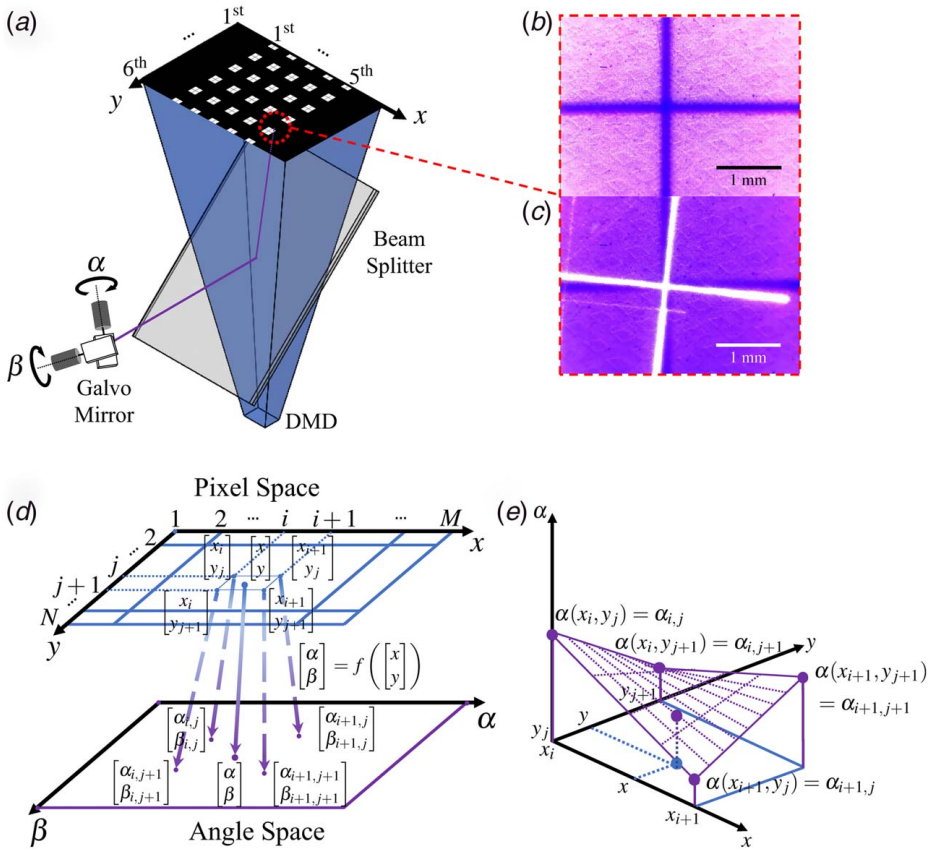

Fig. 5 Calibration mapping from the angular space to the pixel space. (*a*) A 5–6 square-grid points separated by 160 pixels are shown to be mapped by the angular space, which fully covers the building area. (*b*) A projection image under the microscope, which is pinpointed by the scanning laser as shown in (c). These data set would be used to interpolate any point from the pixel space to the laser's angular space shown in (*d*) by bilinear interpolation illustrated in (e) (only α is shown. β values can be interpolated in the same way as α).

same focal length from the projector and constitutes a focal plane, which would be aligned to the fabrication plane where photopolymerization of the liquid resin occurs. However, the energy density of each pixel is orders of magnitude smaller than that of a focused laser beam with a similar size.

The laser scanning method controls exposure by directing the laser beam through a pair of orthogonal mirror galvanometers (abbreviated as galvo). The rotation of each galvo mirror is controlled by a servo motor, which can process and execute a stream of angular position data at a fixed rate. The scanning speed of the laser beam can be controlled by the difference of the adjacent pair of data coordinates in the data stream. Thus, for the same line segment to be scanned, the linearly interpolated data with finer mesh will have a slower scanning speed, which will affect the dosage of the laser to the photosensitive resin. A calibration of dimensional accuracy and light dosage will be discussed.

2.2 Machine Design. In the hybrid-light-source SL process, the optical path and the focal plane of each light source are mutually independent of the other. Since the DMD mirror size and the laser beam size directly determine the resolution of fabrication parts, the alignment of the fabrication plane and the focal points of each light source must be ensured. A beam splitter was used to separate the locations of the two light sources and to merge their focal planes, as shown in Fig. 3.

The DMD-based projection can fabricate the inner portion since it can photo-cure the entire layer simultaneously regardless of its shape complexity. The high-resolution laser beam can be used to draw the contours of each layer, achieving a smoother surface finish [18]. More importantly, the micro-structures on the surface of the part have a single pixel or sub-pixel sizes. They can only be fabricated via the focused laser beam due to its requirements on fine resolution and high intensity. Details of the slicing and toolpath planning algorithms will be discussed in Sec. 3.

The design of the entire machine is shown in Fig. 4. The laser diode has the power of 220 mW and an adjustable lens at the output. A bi-convex lens (N-BK7 from *Thorlabs*) with a focal length of 250 mm was selected to focus the laser beam with enough depth of field. Each galvo mirror has a scanning speed of 30 kilo-points per second (kpps) with travel angle of 12 deg and a resolution of 0.003 deg (4000 steps), covering the circular envelope with the radius of 53 mm (step size of 25 μm). The DMD projector has the projection envelope of 128–80 mm with a pixel resolution of 100 μm. Therefore, the effective build area of the system is the center rectangle of the DMD projection envelope circumscribed by the laser envelope with the size of 76.8–80.0 mm. The thickness of the beam splitter would cause the reflection of the laser beam at the second surface, which forms a so-called "ghost image" at the fabrication plane. However, the energy of the ghost image is much weaker than that of the main beam spot. Based on our tests, the ghost image does not affect fabrication so long as the laser scanning speed is larger than 0.001 m/s, which can be ensured in the laser toolpath planning.

There are four components in our hardware setup that need to be finely adjustable in the hardware system, that is, projector, lens, mirror mounts *A* and *B* (refer to Fig. 4(*a*)). The light projection of a DMD-based projector was focused at the fabrication plane by a

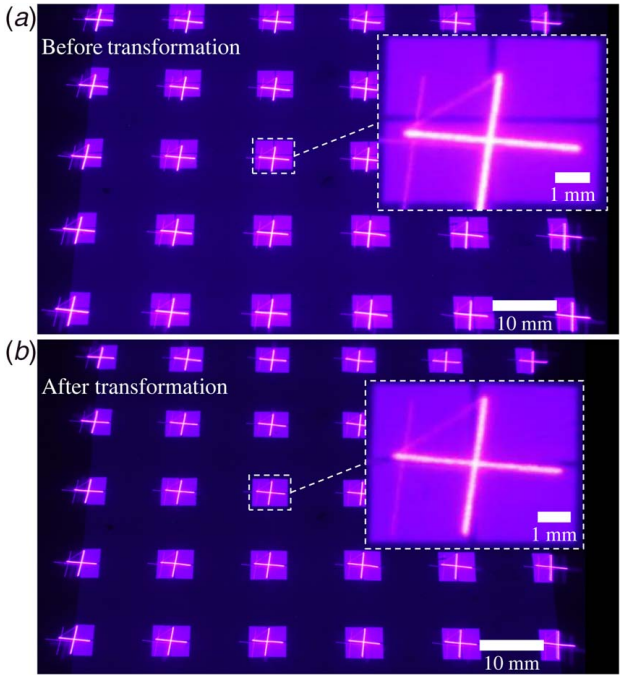

Fig. 6 Mapping of reference data points between the pixel space (four-square array) and the angle space (cross). (*a*) The measurements of the original angular space before correction are shown (with drifted errors). (*b*) The correction effect by the projective transformation is shown. After the correction, the error is no larger than 1 pixel. Note that the pixel space is always fixed, and each photo is taken with 30-second-long exposure to capture the laser scanning through all the reference points.

precision manual stage beneath the top plate. Mirror mounts *A* and *B* were tuned to align the laser beam to the center of the galvo mirror and finely adjust the object distance to the twice of focal length. During the focusing of the laser, the lens can be tuned in *Y*-direction to find the correct image distance (also twice of focal length). Eventually, the beam size can be determined by measuring the width of line features cured by laser scanning. Overall, a mesoscale projection and a 50-μm laser beam were configured in the hybrid SL system to enable multi-scale fabrication.

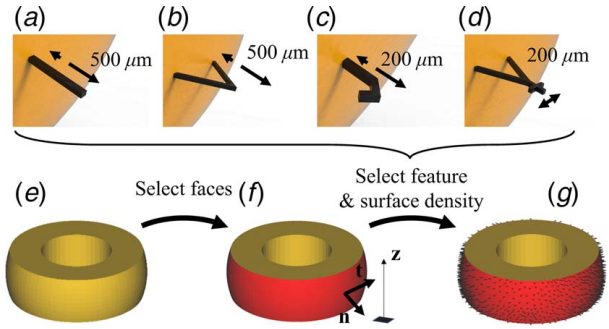

Fig. 8 Design of four types of micro-features with schematics: bar, hook, triangle, and triangle + cross (from left to right at the top) on the input model. The features are attached on the normal direction to the selected face by aligning with the normal vector *n*. The accordingly designed micro-textures with the given surface are shown.

2.3 Calibration. The focal planes of the two independent light sources can be mechanically aligned with the fabrication plane to achieve the smallest curable feature; however, the exact dimensional positioning mapping between these two light sources is difficult to align mechanically due to the image distortions with many degrees-of-freedom. Busetti et al. proposed a calibration method to map positions of two sources [21]. However, the inherent nonlinearity of the galvo mirrors was not concerned as its angular control might not be exactly accurate as predicted, leading to the imperfection at the corners of building area. The environmental disturbance that occurs before the actual manufacturing process, for example, the galvo mirrors being reset to a slightly different angular position once powered-on (zero drift), should be accounted as well. In this paper, a systematic calibration method is introduced to tackle the aforementioned nonlinearity and zero-drifting problems.

The developed calibration method essentially unifies three mutually independent spaces: the physical space on the fabrication plane, the pixel space of the DMD-based projector, and the angular space of the two galvo mirrors. Denote (x, y) as the pixel coordinate at xth column and yth row of the image, and denote (α, β) as the rotational angle coordinate of two galvo mirrors. The pixel space can be calibrated to the physical space using the method proposed by Zhou and Chen [22]. Then the layer information including laser toolpath (Fig. 5) can be fully represented in pixel space by two

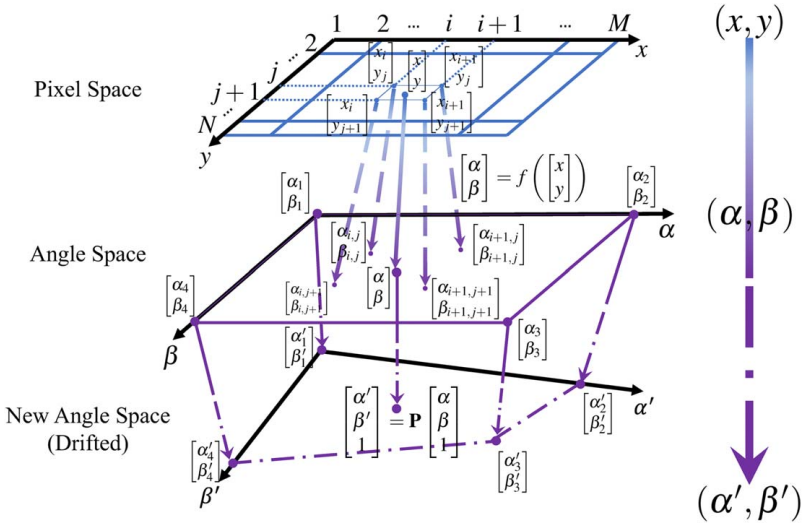

Fig. 7 Complete coordinate transformation diagram: from pixel space to the new angular space with all data points used to transform an arbitrary coordinate (x, y) to (α', β'). The distortion is exaggerated in the new angular space layer.

steps: (1) to construct a fixed bijective function mapping discrete pixel values (x, y) in the pixel space to angular positions (α, β) in the angular space and (2) to set a projective transformation to correct changes in the angular space due to zero drift. These mathematical operations are detailed as follows:

(1) Mapping of pixel space (x, y) to angular space (α, β) with bijective function $(x, y) \mapsto (\alpha, \beta)$

As the focal plane of the pixel space has aligned with the actual fabrication plane, the size of each discrete pixel remains constant (e.g., 100 μm). Denote x-axis as the width of the image and y-axis as the height with the origin set on the top-left corner of the image. Since the galvo mirror demonstrates high nonlinearity, interpolation is used to linearize the mapping bijection. Choose $M \times N$ points that equally divide pixel space into $(M-1) \times (N-1)$ grids and set corners of each grid as reference points. The pixel values of four corners of the (i, j)th grid are denoted as

$$\begin{bmatrix} x_i, y_j & x_{i+1}, y_j \\ x_i, y_{j+1} & x_{i+1}, y_{j+1} \end{bmatrix}$$

Measure angular space coordinates (α_i, β_j) that direct the laser to pass through the corresponding pixel point (x_i, y_j) as shown in Figs. 5(*a*)–5(*c*). Repeat such step for all corners of grids in pixel space to obtain the set of all reference coordinates.

Given the reference points, the mapping of all discrete points can be linearized using bilinear interpolation:

$$\alpha(x, y) = \frac{1}{(x_{i+1} - x_i)(y_{j+1} - y_j)} \times \begin{bmatrix} x_{i+1} - x & x - x_i \end{bmatrix} \begin{bmatrix} \alpha_{i,j} & \alpha_{i+1,j} \\ \alpha_{i,j+1} & \alpha_{i+1,j+1} \end{bmatrix} \begin{bmatrix} y_{j+1} - y \\ y - y_j \end{bmatrix} \tag{1}$$

where (x, y) is the pixel coordinate enclosed in the (i, j)th grid. The mapping for $\beta(x, y)$ has the identical form. The bijection returns the mapped coordinate in the angular space. The more grids we use, the more accurate the result would be.

(2) Zero drift correction of the angular space with projective transformation

The mappings of reference data set $(x, y) \mapsto (\alpha, \beta)$ provide sufficient information for the mapping between the two optical sources. However, occasional zero drift can happen due to the hardware configuration, resulting in the change of angular space and invalidating the original bijection mapping. Remeasuring all $M \times N$ reference points would construct the new bijection; however, it is a laborious method to accommodate the zero drift change. Here, a projective transformation method can be used to correct the linear distortion of angular space. Denote coordinates of newly changed angle space as (α', β'), and the transformation is presented as follows:

$$\begin{bmatrix} \alpha' \\ \beta' \\ 1 \end{bmatrix} = \begin{bmatrix} p_1 & p_4 & p_7 \\ p_2 & p_5 & p_8 \\ p_3 & p_6 & 1 \end{bmatrix} \begin{bmatrix} \alpha \\ \beta \\ 1 \end{bmatrix} = \mathbf{P} \begin{bmatrix} \alpha \\ \beta \\ 1 \end{bmatrix} \tag{2}$$

The eight parameters p_1 to p_8 of transformation matrix $\mathbf{P}$ account for translation, rotation, and projection of original angular space, and they can be solved by plugging four pairs of angle coordinates at four corners of both angular spaces. Only four measurements are required to solve $\mathbf{P}$, and all the original angle coordinates (α, β) can be transformed to the new angular space using the method. Figure 6 shows the correction effect of the transformation.

The information flow of coordinates through the calibration process is summarized in Fig. 7. Besides the dimensional calibration of the system, the energy calibration may also be

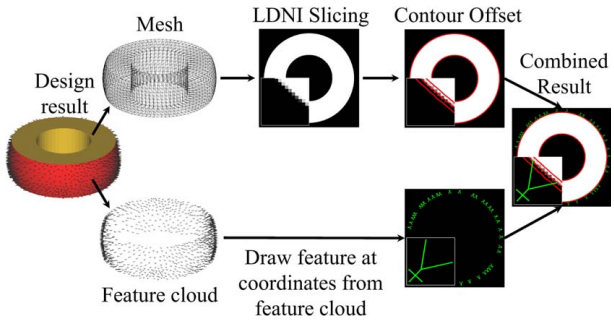

Fig. 9 Projection image and laser toolpath generation from the micro-texture design result, which is separated into the original mesh file and the feature cloud of the micro-textures. The mesh is sliced using LDNI to preserve minimum feature. Laser toolpaths are computed by offsetting layer boundary multiple times inward. Micro-texture features are drawn on the layer with the defined position information from the feature cloud.

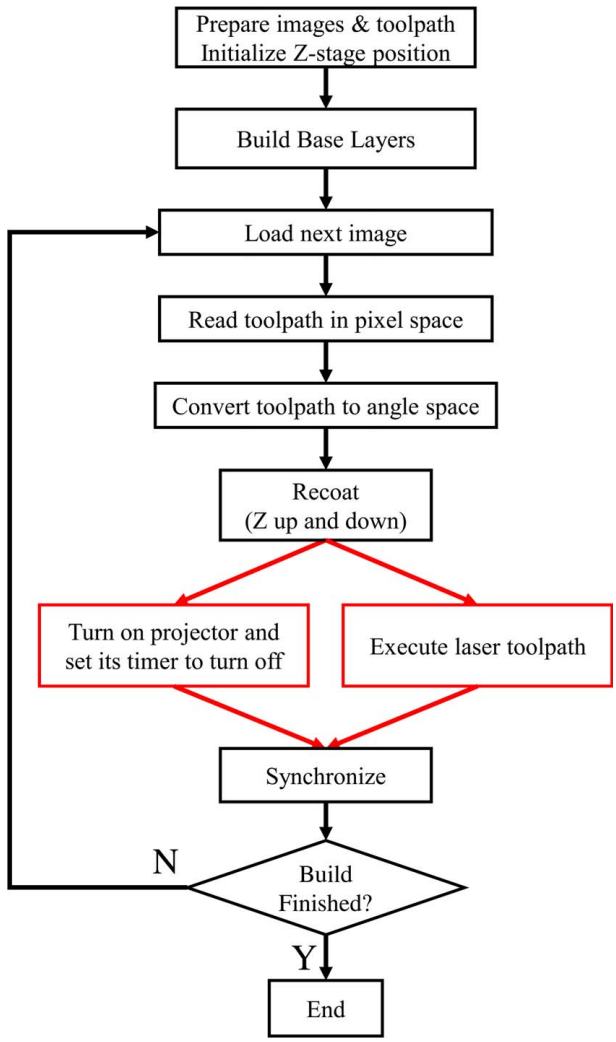

Fig. 10 Flowchart of the build cycle of the proposed parallel hybrid system including a parallel process in the flowchart

performed to ensure a uniform projection and laser power distribution [15]. Based on the hardware design and configuration of the hybrid-light-source SL system, the algorithms of generating mask images and laser toolpaths are discussed in Sec. 3.

3 Process Planning and Micro-Structure Design

The hybrid-light-source SL process combines two types of energy sources in the multi-scale fabrication process. Hence, the individual toolpath information of both projection images and laser tool path need to be integrated to fabricate a given CAD model with multi-scale features. It is challenging to directly process a CAD model with micro-structures. Instead, an additional micro-texture design system was developed to aid in the toolpath planning of the hybrid-light-source SL system. That is, the micro-texture design system takes a uniformly meshed .STL file as the representation of the macroscale 3D object to be fabricated. The micro-structures to be fabricated are defined in the micro-texture design system as pre-defined micro-textures and saved as a micro-texture design file, which is separate from the STL file defined for the macroscale 3D object. Accordingly, the process planning system will automatically generate the mask images for the 3D object and a sequence of laser toolpaths for the layer boundary and micro-structures. The developed algorithms for the hybrid-light-source SL system are discussed in detail in this section.

3.1 Design and Limitation of Micro-Structures. In the design stage, a user has the freedom of specifying the micro-texture types, the surfaces that the micro-textures will attach to, and the density of the micro-textures. Accordingly, a design system will generate the CAD model of the desired micro-textures. Unfortunately, none of such a CAD system exists to our knowledge. In this research, a prototype micro-texture design system was developed for the proof of concept. Four 2.5D micro-textures were predefined in our design system (Figs. 8(*a*)–8(*d*)), which are printable by our multi-scale SL system. For each micro-texture, several degrees of design freedoms including the installation angle and feature length were provided in the design system. A graphical user interface was also developed to enable the selection of surfaces on a mesh model (Figs. 8(*e*) and 8(*f*)). After obtaining the locations of micro-textures, the micro-textures are then distributed on the selected surface via Voronoi tessellation (Fig. 8(*g*)). Their locations and shapes can be saved in a separate file using an internally defined format. Accordingly, the process planning system can plan the toolpath for them on each slicing plane. Details on the toolpath planning of the developed hybrid-light-source SL system will be discussed in the following subsections.

There are a few limitations on the micro-textures that can be designed and fabricated in our system. First, the added micro-textures can only be on the slicing plane and hence 2.5D. Note, due to the small feature sizes, no support structures are considered for the added micro-textures. Hence, a true 3D micro-texture will present significant challenges during the fabrication process. For a given building direction z, a major step to add micro-textures is to find the proper location and orientation by identifying the surface normal of each micro-texture to be inserted to the surface. The contour of the sliced layer is required to determine the vector $\boldsymbol{n}$ normal to the outer surface (Fig. 8(*f*)). As the contour is made up of small segments, the normal vector $\boldsymbol{n}$ can be defined by the cross product of the slice plane normal z and the tangent segment $\boldsymbol{t}$. Based on the normal vector and the designed feature location, different styles of features can be added accordingly. Second, since each micro-texture is required to be self-supported during the fabrication process, the feature cannot be extended outward too long. Our experimental results indicate that micro-structures that extend outward larger than 0.85 mm would begin to result in collapse. To be safe, the maximum feature size of each micro-texture pattern from surface boundary is set to be 0.5–0.7 mm. Third, there is minimum interval distance between neighboring micro-structures. In our system, approximately 0.4 mm is set to guarantee all the features of neighboring micro-textures that can be fabricated separately.

3.2 Multi-Scale Toolpath Planning. Once micro-textures were designed on the object surfaces, the next step is to convert the micro-texture design result to appropriate toolpath for the hybrid SL machine. We first converted the .STL file of the 3D object into a layer depth normal image (LDNI) model such that we can easily identify the cross-sectional area on a slicing plane and create a binary image with a given resolution [23]. The input solid was converted to an LDNI solid S where its minimum features were preserved. The laser beam has a spot size $p = 50\,\mu$m and a step size of $p/2$, the smallest step distance the laser system can achieve. Initially, an image I specifying the cross section is created with the pixel size equal to $p/2$. This is because we want to build the image with fine enough resolution to maintain the toolpath accuracy.

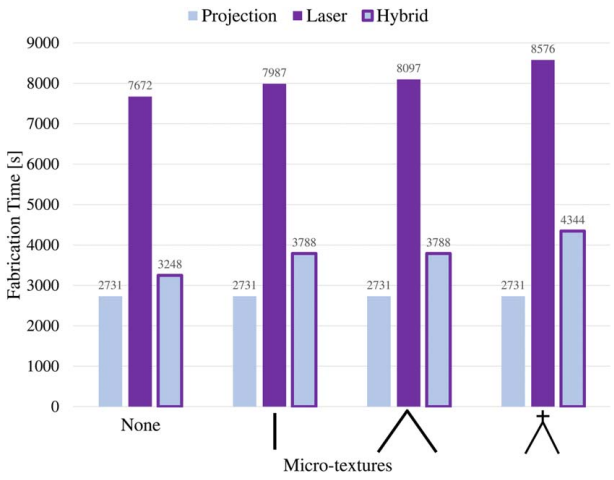

Fig. 11 Time comparison among the processes across various micro-textures. The layer thickness is 50 μm for all the tests. Note that micro-textures are only fabricated on the laser and hybrid tests since they cannot be fabricated by the projection-based system. The reported projection time is only to fabricate the macroscale object. In all the tests, the laser scanning speed is 0.1 m/s for contours and 0.01 m/s for the features of micro-textures.

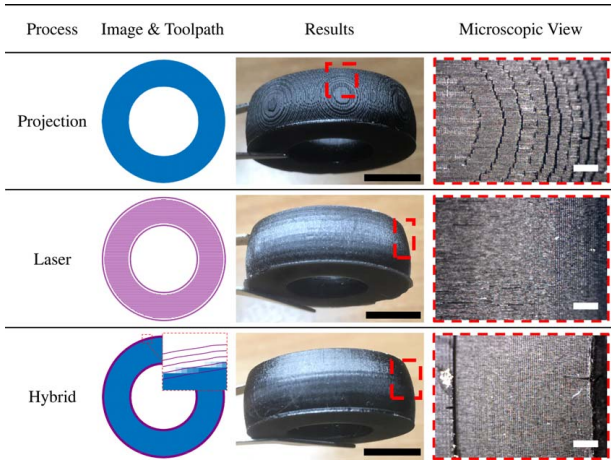

Fig. 12 Fabrication results of the ring model without micro-textures. The hybrid process removes undesired aliasing patterns without losing throughput. In the figures, the black scale bar is 10 mm, and the white scale bar is 500 μm.

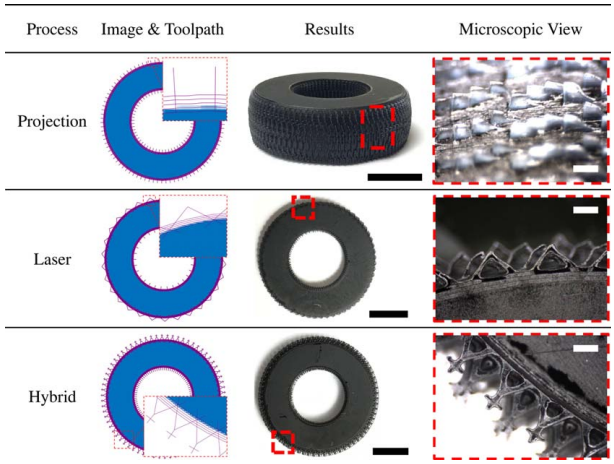

Fig. 13 Fabrication results of the ring model with the micro-textures of bars, triangles, and tri-crosses as shown in Fig. 8. In the figures, the black scale bar is 10 mm, and the white scale bar is 500 μm.

In the next step, a series of shrink offset operation $C(r)$ are applied on I to extract the path region, as shown in Fig. 9. The offset distance is the spot size of the laser beam ($r = -p$) and multiple offsetting are performed for several contour paths. The conversion of mesh model into LDNI model enables us to perform layer boundary offsetting robustly [24]. For every layer contour, the path is located at the boundary edges of the inner pixels after performing $C(p/2)$ on I—that is where the center of the beam should be placed. By connecting the boundary edges and smoothing the connected polygon to avoid the staircase effect in each path region, contour paths are obtained. More details regarding the laser toolpath construction can be found in Ref. [19].

To build an input 3D model, the contour and the micro-features are printed with the laser-based system to achieve detailed surface, while the rest of the cross-sectional area is printed with the high-throughput projector. The exact contour and related offset ensure the connection of micro-texture features and their secure bonding with the layer contours in a slicing plane. With the necessary data provided from software, the next step is to coordinate two independent optical sources that can be controlled simultaneously to maximize the efficiency of the hybrid SL process.

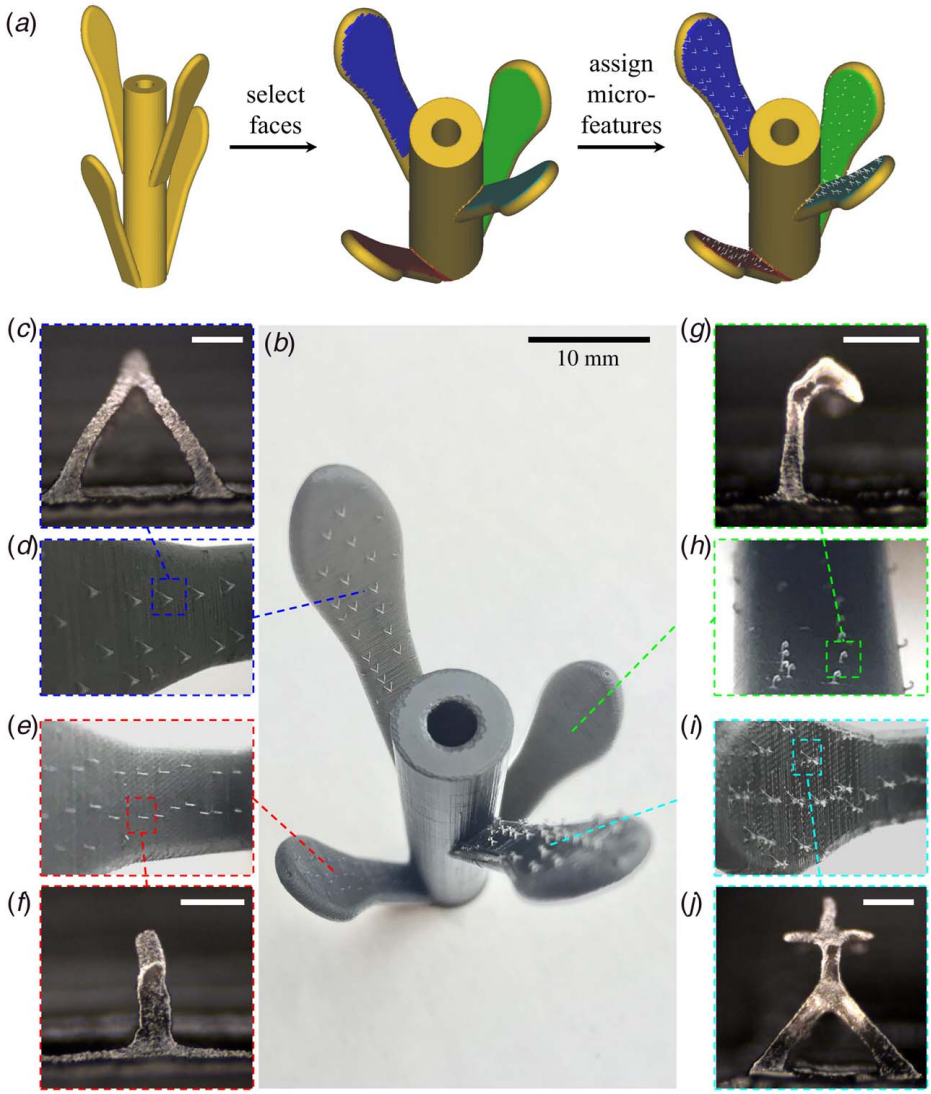

Fig. 14 Stem model with different micro-features distributed on its four leaves. (*a*) The mesh of the stem model, whose surfaces are selected and assigned with unique micro-textures. (*b*) The actual result fabricated by the hybrid-source process. (*c*)–(*j*) Zoomed-in and microscopic pictures of each micro-feature on the leaf surface. The white scale bar is 200 μm.

3.3 Process Planning and Control. While traditional SL process utilizes single light sources to fabricate parts sequentially, the hybrid-source system provides multi-scale sources that can be controlled independently, which provides another degree-of-freedom in designing the parallel manufacturing process. With separate layer information obtained for each scale of the light source, a collaborative parallel process coordinating different tools with different throughputs is used to achieve maximum fabrication efficiency, as presented in Fig. 10.

The developed AM system was controlled by a specially developed C++ program on a host personal computer. It connects with *KMotion* controller for the *Z*-stage motion control, a *Lasershark* board for galvo mirror control, and a projector through high-definition multimedia interface (HDMI) and a serial port. The entire process was characterized by a self-developed "a-code" as a variant of G-code, which contains the minimum information for each action. It would be generated within the laser toolpath file and executed by the control program. The pixel resolution of the projector limits its capability to fabricate micro-feature in macroscale fabrication area. The laser system draws micro-structures well, but it will take a longer time to scan across a large solid inner portion. With the parallel process, the fabrication of the solid part and micro-structures will be performed simultaneously, boosting the efficiency of the manufacturing process. Both hybrid and laser methods were used to fabricate the same solid object with micro-textures, and the results are presented in Sec. 4.

4 Results and Discussion

The hybrid-light-source SL process can fabricate designed macroscale objects using the high-throughput image projection system and the additional microscale surface textures using the high-resolution laser scanning system. Several test cases were designed and fabricated to demonstrate the developed multi-scale SL process.

The first part is a ring that was created by slicing the middle one-third part of a sphere with a diameter of 30 mm. Then a cylindrical through hole was cut at the center of the flat surface (same model in Figs. 2 and 3). The ring model was fabricated with the projection-only, laser-only, and hybrid-light-source SL processes, respectively. Then various types of micro-features were added on the curved surface. The photo-curable resin used in our tests was *MakerJuice*. A comparison of the required fabrication time for the tests is presented in Fig. 11.

The toolpath planning and the fabrication results of the ring models without and with micro-textures are shown in Figs. 12 and 13, respectively. For the solid ring without any micro-textures (Fig. 12), the surface fabricated by the projection-only has undesired aliasing patterns due to the limited *XY* resolution of the projector (refer to the microscopic view in projection process). In contrast, the laser and hybrid methods produce better surface quality due to a higher resolution of the galvo mirror system, which effectively reduces the undesired aliasing patterns. In addition, the hybrid method maintains the same throughput as the projection method, which takes less than half of the time of the laser-only method (refer to the fabrication time in Fig. 11).

For the solid ring with various micro-textures (Fig. 13), the micro-texture features on the ring model require high-resolution energy input and control. The micro-textures cannot be fabricated by the projection-only method due to their small sizes; instead, they can only be fabricated by the laser scanning method. The hybrid-light-source SL process can be over twice faster than the laser-only method for the ring model with various micro-textures. The efficiency advantage of the hybrid method would be even more significant for an object with a larger area and more complex geometric shapes.

Our micro-texture design system enables arbitrary selections of any surface portion on which a micro-texture from the pre-defined library can be added. A solid model can have many different types of micro-textures on different surfaces. A complex test case using a plant stem model with four leaves was designed as shown in Fig. 14. Each of the four micro-textures in our library was added on each surface of its four leaves. In our micro-texture design system, we can also have the full control of micro-texture distribution and density. In the designed plant stem model, the designed micro-textures on each leaf have different distributions and densities. The fabrication of the stem model with micro-textures was efficiently finished with the hybrid-source process, which maintained the high throughput regardless of the complexity of micro-textures, the mesh model, and the specification of the micro-textured regions. The fabrication results are shown in Fig. 14, which demonstrate the full capability of the multi-scale SL process based on hybrid light sources.

5 Conclusion

The hybrid-light-source stereolithography process that integrates both the DMD-based projection method and the laser-based scanning method can fabricate macroscale objects with microscale surface textures effectively and efficiently. A hybrid-light-source SL prototype system has been developed that possesses both high resolution of the laser-based system (50 μm spot size and 25 μm step size) and high throughput of the projection-based method (8 seconds per layer for 50 μm layer thickness regardless of its layer shape). Using the developed multi-scale SL system, a hierarchy of multi-scale geometric complexity can be achieved for a 3D object. The trade-offs of the SL process on fabrication resolution, speed, and area sizes can be better addressed over SL processes using any single light source. Both hardware design and the calibration method of different light sources were discussed. The toolpath planning method based on a micro-texture design system for the hybrid-light-source SL process has also been demonstrated. A library of micro-textures was constructed that can be quickly converted into toolpaths of micro-texture features and integrated in the fabrication of a solid model. For the nature-inspired structures that typically require large-area with fine resolution, the hybrid-light-source SL process will be more effective and efficient than the traditional SL processes.

One major limitation of the developed hybrid-light-source SL system is that it can only build 2.5D micro-structures with limited feature sizes. A true 3D micro-structure could be achieved by selecting more advanced resin, which could form soluble support structures on these fragile micro-features. In addition, the slight deformation of the fragile micro-features can be observed after rinsing and post-processing of the 3D-printed part. These issues will be addressed in our future work. Other planned future work includes the fabrication of biomimetic structures using the developed AM process and performing research on their unique functions on enhancing fluidic, mechanic, biomedical, and electric properties. The hybrid-light-source SL process would enable one to prototype and engineer components with various micro-textures and to assist the future investigation on biomimetic research.

Acknowledgment

The work was partially supported by Sprintray. The first author is grateful for the support of a USC Provost's Undergraduate Research Fellowship and the USC Undergraduate Research Associates Program. The authors also acknowledge Jie Jin and Sabrina Albrecht at USC for their assistance in machine setup and experiments, and Professors Gene Bickers and Matthew Gilpin at USC for their helpful discussions.

Conflict of Interest

There are no conflicts of interest.

Data Availability Statement

The datasets generated and supporting the findings of this article are obtained from the corresponding author upon reasonable request.

References

[1] Wen, L., Weaver, J. C., and Lauder, G. V., 2014, "Biomimetic Shark Skin: Design, Fabrication and Hydrodynamic Function," J. Exp. Biol., **217**(10), pp. 1656–1666.

[2] Oeffner, J., and Lauder, G. V., 2012, "The Hydrodynamic Function of Shark Skin and Two Biomimetic Applications," J. Exp. Biol., **215**(5), pp. 785–795.

[3] Cerman, Z., Striffler, B. F., and Barthlott, W., 2009, *Dry in the Water: The Superhydrophobic Water Fern Salvinia—A Model for Biomimetic Surfaces*, Springer Netherlands, Dordrecht, pp. 97–111.

[4] Barthlott, W., Mail, M., Bhushan, B., and Koch, K., 2017, "Plant Surfaces: Structures and Functions for Biomimetic Innovations," Nano-Micro Lett., **9**(23), pp. 1265–1305.

[5] Yang, Y., Li, X., Zheng, X., Chen, Z., Zhou, Q., and Chen, Y., 2018, "3d-Printed Biomimetic Super-Hydrophobic Structure for Microdroplet Manipulation and Oil/Water Separation," Adv. Mater., **30**(9), p. 1704912.

[6] Yang, Y., Song, X., Li, X., Chen, Z., Zhou, C., Zhou, Q., and Chen, Y., 2018, "Recent Progress in Biomimetic Additive Manufacturing Technology: From Materials to Functional Structures," Adv. Mater., **30**(36), p. 1706539.

[7] Hull, C., 1985, "Apparatus for Production of Three-Dimensional Objects by Stereolithography," U.S. Patent US4575330A.

[8] Lee, M. P., Cooper, G. J. T., Hinkley, T., Gibson, G. M., Padgett, M. J., and Cronin, L., 2015, "Development of a 3D Printer Using Scanning Projection Stereolithography," Sci. Rep., **5**(1), p. 9875.

[9] Emami, M. M., Barazandeh, F., and Yaghmaie, F., 2014, "Scanning-Projection Based Stereolithography: Method and Structure," Sens. Actuators A, **218**(1), pp. 116–124.

[10] Lee, H., and Fang, N., 2012, "Micro 3D Printing Using a Digital Projector and its Application in the Study of Soft Materials Mechanics," J. Visualized Exp., **69**(1), p. 4457.

[11] Spadaccini, C. M., Farquar, G., Weisgraber, T., Gemberling, S., Fang, N., Xu, J., Alonso, M., and Lee, H., 2011, "High Resolution Projection Micro Stereolithography System and Method," U.S. Patent US9492969B2.

[12] Sun, C., Fang, N., Wu, D., and Zhang, X., 2005, "Projection Micro-Stereolithography Using Digital Micro-Mirror Dynamic Mask," Sens. Actuators A, **121**(1), pp. 113–120.

[13] Deubel, M., von Freymann, G., Wegener, M., Pereira, S., Busch, K., and Soukoulis, C., 2004, "Direct Laser Writing of Three-Dimensional Photonic-Crystal Templates for Telecommunications," Nat. Mater., **3**(1), pp. 444–447.

[14] Selimis, A., Mironov, V., and Farsari, M., 2015, "Direct Laser Writing," Microelectron. Eng., **132**(C), pp. 83–89.

[15] Li, X., and Chen, Y., 2017, "Micro-Scale Feature Fabrication Using Immersed Surface Accumulation," J. Manuf. Process., **28**(3), pp. 531–540.

[16] Mao, H., Zhou, C., and Chen, Y., 2016, "LISA: Linear Immersed Sweeping Accumulation," J. Manuf. Process., **24**(2), pp. 406–415.

[17] Zhou, C., Ye, H., and Zhang, F., 2015, "A Novel Low-Cost Stereolithography Process Based on Vector Scanning and Mask Projection for High-Accuracy, High-Speed, High-Throughput, and Large-Area Fabrication," ASME J. Comput. Inf. Sci. Eng., **15**(1), p. 011003.

[18] Ye, H., Zhou, C., and Xu, W., 2017, "Image-Based Slicing and Tool Path Planning for Hybrid Stereolithography Additive Manufacturing," ASME J. Manuf. Sci. Eng., **139**(7), p. 071006.

[19] Mao, H., Leung, Y., Li, Y., Hu, P., Wu, W., and Chen, Y., 2017, "Multi-Scale Stereolithography Using Shaped Beams," ASME J. Micro Nano-Manuf., **5**(4), p. 040905.

[20] Cao, Y., Dichen, L., and Jing, W., 2013, "Using Variable Beam Spot Scanning to Improve the Efficiency of Stereolithography Process," Rapid Prototyp. J., **19**(2), pp. 100–110.

[21] Busetti, B., Steyrer, B., Lutzer, B., Reiter, R., and Stampfl, J., 2018, "A Hybrid Exposure Concept for Lithography-Based Additive Manufacturing," Addit. Manuf., **21**(1), pp. 413–421.

[22] Zhou, C., and Chen, Y., 2012, "Additive Manufacturing Based on Optimized Mask Video Projection for Improved Accuracy and Resolution," J. Manuf. Process., **14**(2), pp. 107–118.

[23] Wang, C., Leung, Y.-S., and Chen, Y., 2010, "Solid Modeling of Polyhedral Objects by Layered Depth-Normal Images on the GPU," Comput. Aided Des., **42**(6), pp. 535–544.

[24] Chen, Y., and Wang, C. C., 2011, "Uniform Offsetting of Polygonal Model Based on Layered Depth-Normal Images," Comput. Aided Des., **43**(1), pp. 31–46.